An Analysis of Entorhinal Cortex Projections to the Dentate Gyrus, Hippocampus, and Subiculum of the Neonatal Macaque Monkey

David G. Amaral,[1]* Hideki Kondo,[1] and Pierre Lavenex[2,3]

[1]Department of Psychiatry and Behavioral Sciences, The M.I.N.D. Institute, The Center for Neuroscience and the California National Primate Research Center, University of California, Davis, Davis, California 95817
[2]Laboratory of Brain and Cognitive Development, Department of Medicine, Fribourg Center for Cognition, University of Fribourg, 1700 Fribourg, Switzerland
[3]Laboratory for Experimental Research on Behavior, Institute of Psychology, University of Lausanne, 1015 Lausanne, Switzerland
[4]Center for Molecular and Behavioral Neuroscience, Rutgers, The State University of New Jersey, Newark, New Jersey 07102

ABSTRACT

The entorhinal cortex is the primary interface between the hippocampal formation and neocortical sources of sensory information. Although much is known about the cells of origin, termination patterns, and topography of the entorhinal projections to other fields of the adult hippocampal formation, very little is known about the development of these pathways, particularly in the human or nonhuman primate. We have carried out experiments in which the anterograde tracers ^{3}H-amino acids, biotinylated dextran amine, and *Phaseolus vulgaris* leucoagglutinin were injected into the entorhinal cortex in 2-week-old rhesus monkeys (*Macaca mulatta*). We found that the three fiber bundles originating from the entorhinal cortex (the perforant path, the alvear pathway, and the commissural connection) are all established by 2 weeks of age. Fundamental features of the laminar and topographic distribution of these pathways are also similar to those in adults. There is evidence, however, that some of these projections may be more extensive in the neonate than in the mature brain. The homotopic commissural projections from the entorhinal cortex, for example, originate from a larger region within the entorhinal cortex and terminate much more densely in layer I of the contralateral entorhinal cortex than in the adult. These findings indicate that the overall topographical organization of the main cortical afferent pathways to the dentate gyrus and hippocampus are established by birth. These findings add to the growing body of literature on the development of the primate hippocampal formation and will facilitate further investigations on the development of episodic memory. J. Comp. Neurol. 522:1485–1505, 2014.

INDEXING TERMS: perforant path; medial temporal lobe; topographical and laminar organization; development; primate

The hippocampal formation is an important component of the medial temporal lobe memory system (Squire et al., 2004). The dentate gyrus, hippocampus, and subiculum in nonhuman primates receive major inputs from the entorhinal cortex via the perforant and alvear pathways (Van Hoesen and Pandya, 1975b; Witter et al., 1989; Witter and Amaral, 1991). The entorhinal cortex, in turn, has prominent bidirectional connections with a variety of polysensory cortical regions including the perirhinal and parahippocampal cortices, orbitofrontal cortex, cingulate and retrosplenial cortices, insula, and polysensory regions of the superior temporal gyrus (Insausti and Amaral, 2008; Lavenex et al., 2002; Mohedano-Moriano et al., 2007, 2008; Suzuki and Amaral, 1994; Van Hoesen and Pandya, 1975a; Van Hoesen et al., 1972). This anatomical organization suggests that the entorhinal

Grant sponsor: National Institutes of Health; Grant numbers: R01-NS16980 (to D.G.A.) and RR00169 (to the California National Primate Research Center, where part of the work was conducted); Grant sponsor: The Swiss National Science Foundation; Grant numbers: PP00A-106701 and PP00P3-124536 (to P.L.).

*CORRESPONDENCE TO: David G. Amaral, Ph.D., The M.I.N.D. Institute, University of California, Davis, 2825 50th Street, Sacramento, CA 95817. E-mail: dgamaral@ucdavis.edu

Received January 15, 2013; Revised September 7, 2013;
Accepted September 13, 2013.
DOI 10.1002/cne.23469
Published online October 1, 2013 in Wiley Online Library (wileyonlinelibrary.com)

cortex plays an important role as an interface between higher order sensory neocortical areas and several fields of the hippocampal formation (Lavenex and Amaral, 2000).

Previous neuroanatomical studies in adult animals have provided a detailed description of the topographic organization of the projections from the entorhinal cortex to the dentate gyrus, hippocampus, and subiculum in various species including the monkey (Van Hoesen and Pandya, 1975b; Witter and Amaral, 1991; Witter et al., 1989), rat (Amaral and Witter, 1989; Blackstad, 1958; Dolorfo and Amaral, 1998; Hjorth-Simonsen and Jeune, 1972; Ruth et al., 1982, 1988; Steward, 1976; Steward and Scoville, 1976; Tamamaki, 1997; Tamamaki and Nojyo, 1993; Witter, 1993, 2007; Witter et al., 1988; Wyss, 1981), cat (Ino et al., 1998; van Groen et al., 1986; Witter and Groenewegen, 1984), and mouse (van Groen et al., 2003). Projections to the dentate gyrus, and the CA3 and CA2 fields of the hippocampus originate mainly from cells in layer II of the entorhinal cortex, whereas projections to CA1 and the subiculum originate mainly from layer III cells (Witter and Amaral, 1991; Witter et al., 1989). The projections from the entorhinal cortex terminate in the outer two-thirds of the molecular layer of the dentate gyrus, the stratum lucunosum-moleculare of the hippocampus, and the molecular layer of the subiculum (Witter and Amaral, 1991; Witter et al., 1989). Lateral portions of the entorhinal cortex project to caudal levels of the dentate gyrus and hippocampus, whereas medial portions of the entorhinal cortex project to rostral levels (Witter and Amaral, 1991; Witter et al., 1989). Entorhinal cortex projections to the dentate gyrus terminate in a laminar fashion depending on the rostrocaudal location of the cells of origin. Rostral entorhinal cortex projects more heavily to the outer portion of the molecular layer of the dentate gyrus, whereas caudal entorhinal cortex projects more heavily to the middle molecular layer (Witter and Amaral, 1991). In addition, projections from rostral portions of the entorhinal cortex terminate at the border of CA1 and the subiculum, whereas projections from caudal portions of the entorhinal cortex terminate in the portion of CA1 closer to CA2 and in the portion of the subiculum closer to the presubiculum (Witter and Amaral, 1991).

There are very few studies on the development of the entorhinal cortex projections to the other hippocampal fields in any species. The early cytoarchitectonic maturation of the human entorhinal cortex has been described by Kostovic et al. (1993). Entorhinal cortex projections to the hippocampal fields and the subiculum in the human are observed by 19–22 weeks of gestation (Hevner and Kinney, 1996), although there is no available evidence concerning the subsequent maturation of these fiber projections. There are currently no articles on this topic in the macaque monkey. We sought to determine, therefore, the level of maturity of the entorhinal cortex projections to the dentate gyrus, hippocampus, and subiculum in the neonatal macaque monkey. By placing injections of anterograde tracers at several locations within the neonatal entorhinal cortex, we used qualitative neuroanatomical techniques to answer the following specific questions: To what extent are the entorhinal cortex projections observed in the adult macaque monkey also identifiable in the 2-week-old infant? And, are the various topographic gradients of fiber distribution also established by this age? The answers to these questions provide new information that, along with recent quantitative neuroanatomical (Jabes et al., 2010, 2011), genetic (Favre et al., 2012a,b; Lavenex et al., 2011) and behavioral (Lavenex and Lavenex, 2006) studies, provide a clearer understanding of the neurobiological underpinnings for the development of the capacity for episodic or spatial-relational memory in the nonhuman primate.

MATERIALS AND METHODS

Surgery

All surgical and experimental procedures were approved by the University of California Davis Animal Care and Use Committee and conform to NIH guidelines. Seventeen 2-week-old *Macaca mulatta* monkeys of either sex were used in these studies. Two weeks proved to be the earliest age at which the skull could be successfully held within the stereotaxic device. Although our ability to detect sex differences in entorhinal cortex projections was limited in these qualitative, light microscopic studies, we did not observe systematic differences in density of projections or topographic or laminar organization. To compare the results between infants and adults, we also examined cases from a library of entorhinal cortex injections in adult monkeys. Adult animals were of both sexes and ranged from approximately 3 to 6 years of age. Rhesus monkeys reach sexual maturity at approximately 3–4 years of age, and the entorhinal cortex pathways are presumably stable at this age. Experimental procedures for the adult animals were described previously (Chrobak and Amaral, 2007; Suzuki and Amaral, 1994; Witter and Amaral, 1991; Witter et al., 1989), and results from these experiments have been presented in these publications.

For all infant monkeys, magnetic resonance imaging (MRI) scans were performed prior to surgery to define the coordinates for tracer injections. Monkeys were

anesthetized with ketamine hydrochloride (15 mg/kg i.m.) and medetomidine (25–50 μg/kg), intubated with a tracheal cannula, and placed in an MRI-compatible stereotaxic apparatus (Crist Instruments, Damascus, MD). Brain images were acquired on a General Electric (Fairfield, CT) 1.5-T Gyroscan magnet 1-mm-thick sections were acquired by using a T1-weighted inversion recovery pulse sequence (TR = 21, TE = 7.9, NEX 3, FOV = 8 cm, matrix 256 × 256). The MRI images were used to determine the coordinates for injection of the neuroanatomical tracers. The animals remained in the stereotaxic apparatus through the remainder of the surgical procedure to ensure the proper placement of the injections. Animals were transported from the MRI suite to the surgery suite of the California National Primate Research Center, where they were mechanically ventilated and maintained at a surgical level of anesthesia with a combination of isoflurane (1%) and fentanyl (7–10 μg/kg/h). Using sterile procedures, the skull was exposed and a small hole was made at a site appropriate for the injection. Electrophysiological recordings were performed to confirm the appropriate dorsoventral coordinate for placement of the injection (Lavenex et al., 2004). Neuroanatomical tracers were injected iontophoretically or with an air-pressure system (see below). After the last injection, the wound was sutured in three layers and the animal recovered from anesthesia in an incubator under the care and supervision of a specialized primate veterinarian. The animal was returned to its mother once it was fully alert. Analgesics (0.15 mg/kg of oxymorphone given three times daily; or buprenorphine 0.02 mg/kg twice daily) were administered immediately postsurgically. A prophylactic regime of antibiotics (20 mg/kg of cefazolin, three times daily) was also administered during the first 5 days of the survival period.

Neuroanatomical tracer injections

Twelve infant monkeys received injections of ^{3}H-amino acids as an anterograde tracer into the entorhinal cortex. The ^{3}H-amino acid injections consisted of a single injection of 50–100 nl of a 1:1 mixture of [^{3}H]leucine and [^{3}H]proline (concentrated to 100 μCi/μl). The injection was done through glass micropipettes by using air-pressure pulses (Amaral and Price, 1983).

Five additional monkeys received up to two anterograde tracer injections of either *Phaseolus vulgaris* leucoagglutinin (PHA-L; Vector, Burlingame, CA; 2.5% solution in 0.1 M PO_{44} buffer, pH 7.4; $n = 7$), biotinylated dextran amine (BDA; Molecular Probes, Eugene, OR; 10% solution in 0.1 M PO_4 buffer, pH 7.4; $n = 7$), or Fluoro Ruby (FR; Molecular Probes; 10% solution in 0.1 M PO_4 buffer, pH 7.4) into different rostrocaudal and transverse portions of the entorhinal cortex. All these tracer substances were iontophoretically injected (30–45-minute injections with 5 μAmp DC pulses; 7 seconds ON, 7 seconds OFF) through glass micropipettes (20–30-μm tips). These animals also received up to two injections of retrograde tracers that are not germane to the results of the current study and will not be described further.

Following injection of the tracer, the pipette was withdrawn in a manner designed to minimize leakage along the pipette tract. Animals survived for 7 days, were deeply anesthetized with sodium pentobarbital (50 mg/kg i.v., Fatal-Plus, Vortech Pharmaceuticals, Dearborn, MI), and perfused transcardially with ice-cold 1% and 4% paraformaldehyde in 0.1 M phosphate buffer (pH 7.4) following our standard laboratory protocol (Lavenex et al., 2009). The brains were postfixed for 6 hours in the same fixative, cryoprotected in 10% and 20% glycerol solutions in 0.1 M phosphate buffer (pH 7.4; for 24 and 72 hours respectively), rapidly frozen in isopentane, and stored at −70°C until sectioning. Sections were cut at 30 μm on a freezing, sliding microtome and processed for visualization of the tracer substances.

Tissue processing

Sections collected for the analysis of the ^{3}H-amino acid injections were processed according to the protocol of Cowan et al. (1972) for autoradiographic demonstration of the anterogradely transported isotope. Sections were counterstained with thionin to allow the determination of cytoarchitectonic boundaries of different cortical areas (Lavenex et al., 2002).

For BDA, PHA-L, and FR, free-floating sections were processed with constant agitation, at room temperature (unless specified otherwise), for the detection of the transported substance (Lavenex et al., 2004). Immunohistochemistry for PHA-L and FR was carried out as follows. Sections were rinsed 3X 10 minutes in 0.02 M potassium phosphate-buffered saline (KPBS; pH 7.4), incubated for 15 minutes in 0.5% H_2O_2, washed 6X 5 minutes in 0.02 M KPBS, and incubated for 4 hours in a blocking solution made of 0.5% Triton X-100 (TX-100; Fisher Scientific, Pittsburgh, PA), 5% normal goat serum (NGS; Chemicon, Temecula, CA) in 0.02 M KPBS. Sections were then incubated for 40 hours at 4°C in a solution containing a primary antibody against the tracer substance (rabbit anti-PHA-L at 1:12,000 from Vector, rabbit anti-Fluoro Ruby at 1:40,000 from Molecular Probes in 0.3% TX-100, 2% NGS in 0.02 M KPBS). After incubation in primary antiserum, sections were washed 3X 10 minutes in 0.02 M KPBS containing 2% NGS and incubated for 1 hour in a solution containing a biotinylated secondary antibody against rabbit (goat

anti-rabbit IgG at 1:227 from Vector in 0.3% TX-100, 2% NGS in 0.02 M KPBS).

Sections were rinsed 3X 10 minutes in 0.02 M KPBS containing 2% NGS and incubated for 45 minutes in a solution containing an avidin–biotin complex (Biomeda Biostain Super ABC Kit, Middleton, WI) in 0.02 M KPBS. Sections were rinsed 3X 10 minutes in 0.02 M KPBS containing 2% NGS and incubated for another 45 minutes in the solution containing the biotinylated secondary antibody (goat anti-rabbit IgG at 1:227 with 0.3% TX-100, 2% NGS in 0.02 M KPBS). Sections were rinsed 3X 10 minutes in 0.02 M KPBS (with no NGS) and incubated for another 30 minutes in the solution containing the avidin–biotin complex. Sections were rinsed 3X 10 minutes in 50 mM Tris buffer (pH 7.4) and incubated for 45 minutes in a 3,3′-diaminobenzidine (DAB) solution containing 0.05% DAB (0.5 mg/ml of DAB, Fisher Scientific) and 0.04% H_2O_2 in Tris buffer. Finally, sections were rinsed 2X 10 minutes in Tris buffer, 1X 10 minutes in 0.02 M KPBS, mounted on gelatin-coated slides, and dried at 37°C overnight. The mounted sections were then processed for intensification of the DAB reaction product.

Sections were defatted 2X 2 hours in a mixture of chloroform–ethanol (50:50, v/v), hydrated through a graded series of ethanol solutions (2 minutes each in 100%, 100%, 95%, 70%, 50% EtOH), and rinsed in running dH_2O for 10 minutes. Sections were incubated for 40 minutes in a 1% silver nitrate solution (in dH_2O) at 56°C (protected from light), and rinsed in running dH_2O for 10 minutes (protected from light). Sections were incubated for 10 minutes in 0.2% gold chloride (in dH_2O) at room temperature and rinsed in running dH_2O for 10 minutes (protected from light). Sections were stabilized in 5% sodium thiosulfate (in dH_2O) at room temperature for 15 minutes (protected from light) and rinsed in running dH_2O for 10 minutes. Finally, sections were dehydrated through a graded series of ethanol solutions (4 minutes each in 50%, 70%, 95%, 100%, 100% EtOH), and cleared with xylene (3X 4 minutes in 100% xylene); then the slides were coverslipped with DPX (BDH Laboratory Supplies, Poole, UK).

BDA processing was as follows. Sections were rinsed 3X 10 minutes in 0.02 M KPBS, incubated for 15 minutes in 0.5% H_2O_2, washed 6X 5 minutes in 0.02 M KPBS, and incubated for 1 hour in a solution comprised of 1% Triton X-100 (TX-100; Fisher Scientific) in 0.02 M KPBS. Sections were then incubated overnight at 4°C in a solution made up of an avidin–biotin complex (Biomeda Biostain Super ABC Kit), with 0.3% TX-100 in 0.02 M KPBS. Sections were rinsed 3X 10 minutes in 50 mM Tris buffer and incubated for 45 minutes in a DAB solution containing 0.05% DAB, 0.015% H_2O_2 in Tris buffer. Sections were rinsed 2X 10 minutes in Tris buffer, 1X 10 minutes in 0.02 M KPBS, mounted on gelatin-coated slides, and maintained at 37°C overnight. The mounted sections were then processed for intensification of the DAB reaction product and coverslipped as described previously. A 1-in-8 series of sections was counterstained with 0.25% thionin to aid in the definition of cytoarchitectonic boundaries.

Data analysis

The distribution of anterogradely labeled fibers and terminals through the entire rostrocaudal extent of the dentate gyrus, hippocampus, and subiculum was analyzed by using darkfield optics. The boundaries of the subdivisions of the entorhinal cortex were microscopically determined following the nomenclature of Amaral et al. (1987) through analysis of the Nissl-stained series of adjacent sections. To represent the gradients of fiber termination in the dentate gyrus, hippocampus, and subiculum, low-magnification photomicrographs were taken of representative sections for each case. Photomicrographs were taken by using either a LEITZ DMRD microscope, a BetterLight Model 4000E line scanner or a Leica Wild MZ8 Model DFC 280 digital camera system. Photomicrographs were digitally altered by using Adobe Photoshop CS5 (Adobe Systems, San Jose, CA) to improve image contrast and to eliminate artefacts present on the microscope slides.

RESULTS

Cytoarchitecture of the entorhinal cortex and hippocampal formation in infant monkeys

Figure 1 presents coronal sections through the rostrocaudal extent of the entorhinal cortex (A–D) and the other fields of the hippocampal formation (E,F) in a 3-week-old rhesus monkey. The nomenclature and cytoarchitectonic subdivisions have been described previously for the entorhinal cortex (Amaral et al., 1987) and for the hippocampal formation (Amaral et al., 1984; Amaral and Lavenex, 2007; Pitkanen and Amaral, 1993) in adult monkeys. Although there are subtle differences in the packing density and cross-sectional areas of certain hippocampal fields in the neonatal monkey (Lavenex et al., 2007), the various cytoarchitectonic fields and even the borders of each of the fields can be readily identified in the neonatal tissue.

Injection sites

A summary of the locations and relative sizes of all the injections evaluated in this study is presented in Figure 2. Successful injections sampled much of the rostrocaudal and mediolateral extent of the entorhinal cortex.

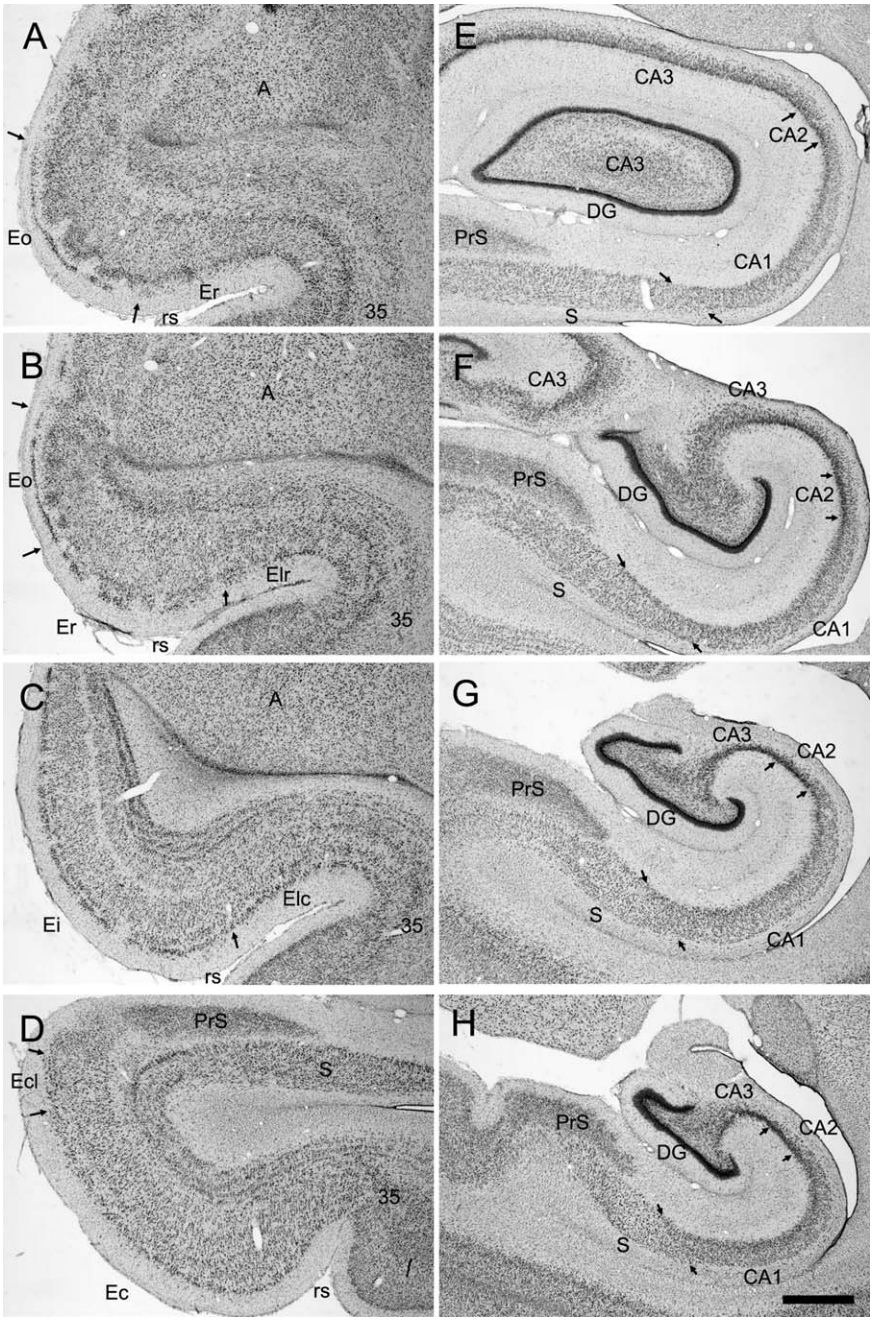

Figure 1. Photomicrographs of Nissl-stained coronal sections of the 3-week-old infant monkey entorhinal cortex (**A–D**) and hippocampal formation (**E–H**). The sections are arranged from rostral (top) to caudal (bottom). The illustration is used to demonstrate the cytoarchitectonic characteristics of the neonatal macaque monkey hippocampal formation at different rostrocaudal levels. Abbreviations: Eo, olfactory field of the entorhinal cortex; Er, rostral field of the entorhinal cortex; Elr, rostral part of the lateral field of the entorhinal cortex; Elc, caudal part of the lateral field of the entorhinal cortex; Ei, intermediate field of the entorhinal cortex; Ec, caudal field of the entorhinal cortex; Ecl, caudal limiting field of the entorhinal cortex; CA1, CA2, CA3, fields of the hippocampus; DG, dentate gyrus; PrS, presubiculum; S, subiculum; rs, rhinal sulcus; A, amygdala; 35, area 35 of the perirhinal cortex. Small arrows indicate boundaries between indicated fields. Scale bar = 1 mm in H (applies to A–H).

Projections: ^{3}H-amino acid injections in the adult entorhinal cortex

The experiments in which ^{3}H-amino acid injections were placed into the neonatal entorhinal cortex provided the clearest demonstration of the overall distribution and topography of the perforant path projections. Previous studies using the autoradiographic method have provided detailed descriptions of the

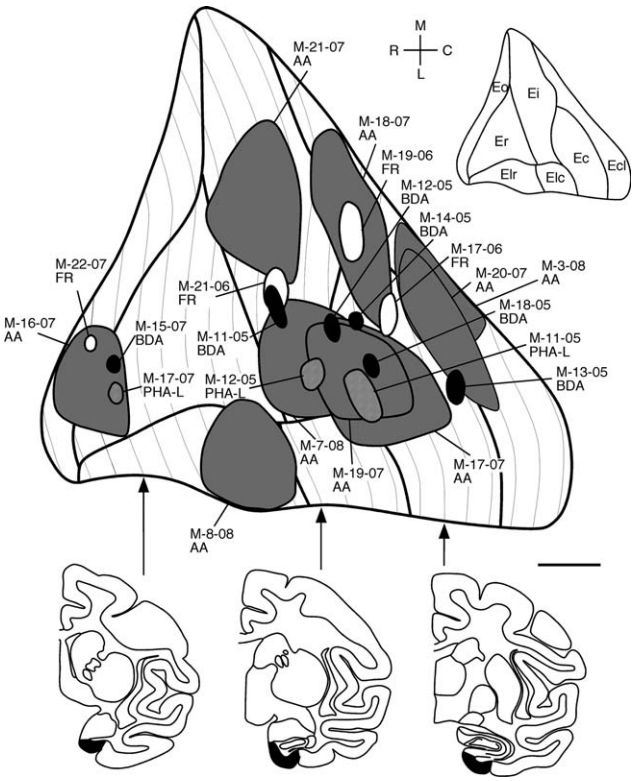

Figure 2. An unfolded, two-dimensional map of the entorhinal cortex illustrating the locations of the anterograde tracer injections into the neonatal monkey entorhinal cortex analyzed in this study. ^{3}H-amino acid injections are illustrated as dark gray profiles, PHA-L injections as profiles with a hatching pattern, BDA injections as black profiles, and FR injections as white profiles. The insert at top right illustrates the different subdivisions of the entorhinal cortex. Mediolateral and rostrocaudal directions are also indicated. Individual injection sites are described in the text. Representative coronal line drawings are shown at three different rostrocaudal levels. AA, ^{3}H-amino acid injections; BDA, biotinylated dextran amine injections; FR, Fluoro Ruby injections; PHA-L, *Phaseolus vulgaris* leucoagglutinin injections. Other abbreviations as in Figure 1 legend. Scale bar = 1 mm.

organization of the perforant path projections in the mature macaque monkey (Witter and Amaral, 1991; Witter et al., 1989). We re-evaluated the same cases used in Witter et al. (1989) and Witter and Amaral (1991) as a basis for comparison with the infant cases. Figure 3 presents low-magnification darkfield images from one adult experiment (M-28-92) in which the ^{3}H-amino acid injection was placed into the most lateral aspect of the lateral field of the entorhinal cortex (Fig. 3A). Labeled fibers could be followed from the level of the injection site, through the angular bundle located subjacent to the entorhinal cortex, and entering the hippocampus through the perforant path (Fig. 3B–D). Labeled fibers heavily innervated the molecular layer of the subiculum, the stratum lacunosum-moleculare of the hippocampus (Fig. 3D), and the molecular layer of the dentate gyrus (Fig. 3E–G). As described in previous studies (Witter and Amaral, 1991; Witter et al., 1989), this laterally placed injection led to the heaviest labeling of caudal levels of the dentate gyrus, hippocampal fields, and subiculum (Fig. 3F–H). Rostral levels (Fig. 3B,C) received very little anterograde labeling. Also typical for a rostrally placed injection, fiber and terminal labeling was heaviest in the outer third of the molecular layer (Fig. 3F,G) and at the border of CA1 and the subiculum (Fig. 3D, asterisk).

Although it is beyond the scope of this article to provide an extensive summary of the topographic organization of the perforant path projections, suffice it to say that there are clear topographic patterns of perforant path termination that are characteristic of the mature entorhinal projections. We evaluated the neonatal cases with entorhinal injections to determine whether these characteristic patterns of termination are apparent in the newborn macaque monkey.

Projections: ^{3}H-amino acid injections in the infant entorhinal cortex

A summary of the relative sizes and locations of the successful ^{3}H-amino acid injections is presented on an unfolded map of the entorhinal cortex (Fig. 2, dark gray profiles). In total, nine ^{3}H-amino acid injections involved some portion of the rostrocaudal and mediolateral extent of the infant entorhinal cortex. An overview of the labeling observed at a mid-rostrocaudal level of the hippocampus resulting from these injections is shown in Figure 4 from case M-17-07. As in adults, all neonatal injections resulted in labeling in the outer two-thirds of the molecular layer of the dentate gyrus, in the full radial extent of stratum lacunosum-moleculare of the hippocampus, and throughout much of the molecular layer of the subiculum (Fig. 4B). Labeled fibers from the entorhinal cortex traveled caudally within the angular bundle, perforated the subiculum, and distributed to terminal regions (Fig. 4B). One pathway that appeared to be much more substantial was the component that traveled within the alveus and then entered the fimbria (Fig. 4B, white arrowheads). We shall return to a description of these fibers when we discuss the commissural connections.

The topographic and laminar organization of the perforant path projection is established in the neonatal macaque monkey

Based on analysis of all of the ^{3}H-amino acid injections, we found that the main features of the topographic and laminar organization observed in the adult

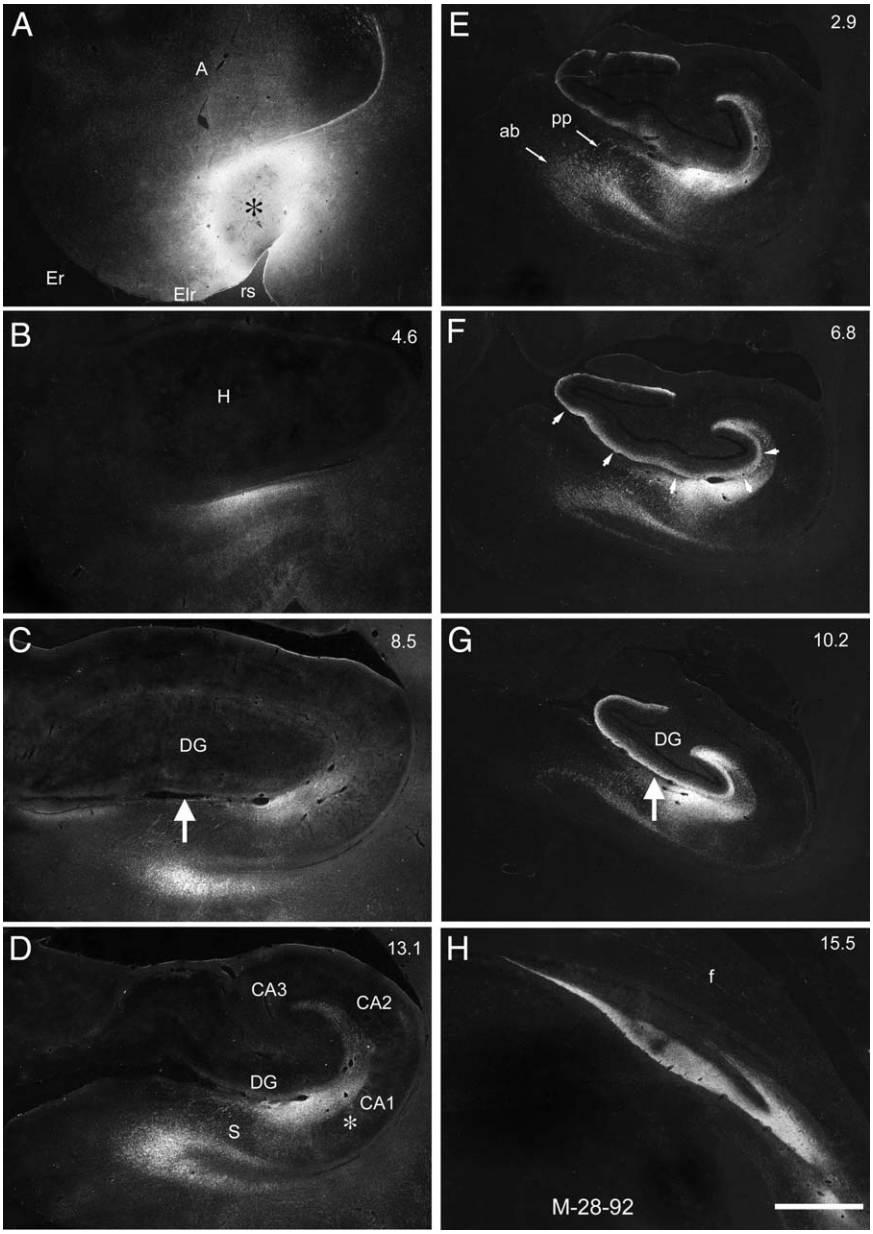

Figure 3. **A–H:** Darkfield photomicrographs of autoradiograms from experiment M-28-92 conducted in an adult macaque monkey. Sections are arranged from rostral (A) to caudal (H). Numbers in the top right of each panel indicate the rostrocaudal distance (in mm) away from the injection site. The injection site is shown in A (black asterisk) and involved all layers of the lateral part of the rostral part of the lateral field of the entorhinal cortex (Elr). Because the injection is placed in the lateral portion of the entorhinal cortex, the heaviest labeling of the molecular layer of the dentate gyrus (DG; indicated with white arrows in F) is found at caudal levels (compare C and G at large white arrows). Although labeling is distributed throughout the outer two-thirds of the molecular layer of the dentate gyrus, it is heaviest in the outer third, consistent with a rostrally placed injection site. There is additional labeling in the stratum lacunosum-moleculare of CA1, CA2, and CA3, and the molecular layer of the subiculum (S). Again, consistent with a rostrally placed injection, the projection to CA1 and the subiculum is distributed most heavily at the border between the two fields (white asterisk, D). The projections from the entorhinal cortex travel caudally from the level of the injection in the angular bundle (ab in E) and perforate the subiculum as the perforant path (pp in E) to enter the molecular layer of the subiculum and stratum lacunosum-moleculare of CA1. Abbreviations: f, fimbria; H, hippocampus. Scale bar = 1 mm in H (applies to A–H).

hippocampal formation are established in the 2-week-old macaque monkey. We present some representative cases to illustrate the maturity of the entorhinal cortex projection system at this age. In case M-17-07 (Fig. 5), the ^{3}H-amino acid injection was located slightly lateral to the mid-transverse portion of the entorhinal cortex, involving the caudal part (Ec), intermediate field (Ei), and caudal part of the lateral field (Elc) at different

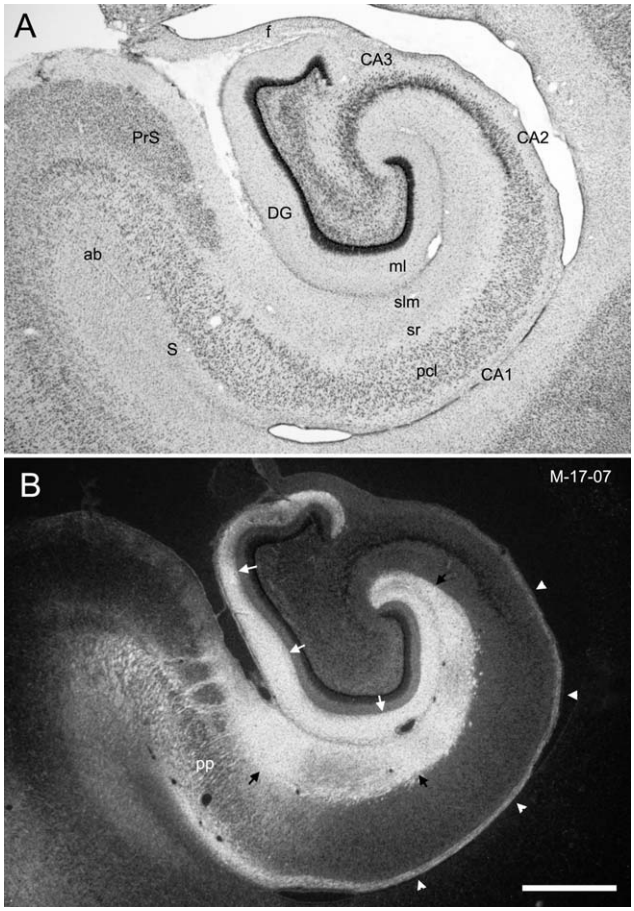

Figure 4. Overview of the entorhinal cortex projections to the dentate gyrus, hippocampus, and subiculum in the 2-week-old infant monkey. **A:** Brightfield photomicrograph of a Nissl-stained coronal section of the hippocampal formation at a mid-rostrocaudal level. **B:** Darkfield photomicrograph of a coronal section adjacent to the one in A showing anterograde labeling following an injection in the lateral part of Ec (case M-17-07; see the injection site in Fig. 5A). Note that labeling is present in the outer two-thirds of the molecular layer of the dentate gyrus (white arrows), the stratum lucunosum-moleculare of CA1, CA2, and CA3, and the molecular layer of the subiculum (black arrows). Projections from the entorhinal cortex perforate the subiculum (pp) to terminate in the hippocampal formation. Arrowheads indicate labeled fibers in the alveus that continue into the fimbria at more caudal levels and contribute to the commissural projections to the contralateral entorhinal cortex. For abbreviations, see Figure 1 legend. Additional abbreviations: ab, angular bundle; ml, molecular layer; pcl, pyramidal cell layer; pp, perforant path; slm, stratum lacunosum-moleculare; sr, stratum radiatum. Scale bar = 1 mm in B (applies to A,B).

rostrocaudal levels (Fig. 5A). Anterogradely labeled fibers and terminals were distributed throughout the entire longitudinal extent of the hippocampal formation except for the uncal portion (i.e., the most medial and rostral part of the hippocampus; Fig. 5B–H). The densest labeling was observed at mid-rostrocaudal levels of the hippocampal formation (Fig. 5D,E). Labeling was substantially weaker at very rostral and very caudal levels (Fig. 5B and H, respectively). In the dentate gyrus, anterogradely labeled fibers were distributed throughout the outer two-thirds of the molecular layer. However, typical of a caudally placed injection, the density of fiber and terminal labeling was noticeably higher in the middle third of the molecular layer (Fig. 5D,5E). In CA1 and the subiculum, the densest patches of labeling were at mid-transverse locations within the fields, as is observed in adult monkeys (Witter and Amaral, 1991; Witter et al., 1989).

The injection in case M-21-07 (Fig. 6A) was at about the same rostrocaudal level of the entorhinal cortex as case M-17-07. However, the injection involved the medial half of the entorhinal cortex rather than the lateral half. Whereas the laminar and regional patterns of termination were similar in M-21-07 as in M-17-07, the projections more heavily terminated at rostral levels of the recipient fields rather than caudal levels (cf. Fig. 6B,C and F–H). These findings are consistent with the results of Witter et al. (1989) and Witter and Amaral (1991): that the medial portion of the entorhinal cortex projects preferentially to rostral levels of the hippocampal formation, whereas the lateral portion projects preferentially to the caudal hippocampal formation.

Laminar differences in the dentate gyrus and CA3, and regional differences in CA1 and the subiculum are observed in the adult depending on the rostrocaudal location of the injection site. Again, this organization was observed in the neonatal macaque monkey, as illustrated in Figure 7, which provides a direct comparison of cases M-16-07 and M-20-07. In case M-16-07 (Fig. 7A–D), the ^{3}H-amino acid injection was located at the rostral pole of the entorhinal cortex and involved the rostral part (Er) and olfactory field (Eo; Fig. 7A). Labeling was observed along the entire longitudinal extent of the hippocampal formation. As would be expected from the pattern observed in adults, labeling in the molecular layer of the dentate gyrus was much heavier in its outer third (Fig. 7B–D). Similarly, the projection was densest at the border of CA1 and the subiculum (Fig. 7C, asterisk). In contrast to case M-16-07, the ^{3}H-amino acid injection in case M-20-07 was located in the caudal limiting field of the entorhinal cortex (Ecl) (Fig. 7E). The projections again terminated throughout the full rostrocaudal extent of the hippocampal formation. However, in contrast to case M-16-07, the heaviest labeling within the dentate gyrus was situated in the middle third of the molecular layer (Fig. 7F–H). Moreover, labeling was densest in the proximal portion of CA1, i,e., closer to CA2, and the distal portion of the subiculum, i.e., closer to the presubiculum

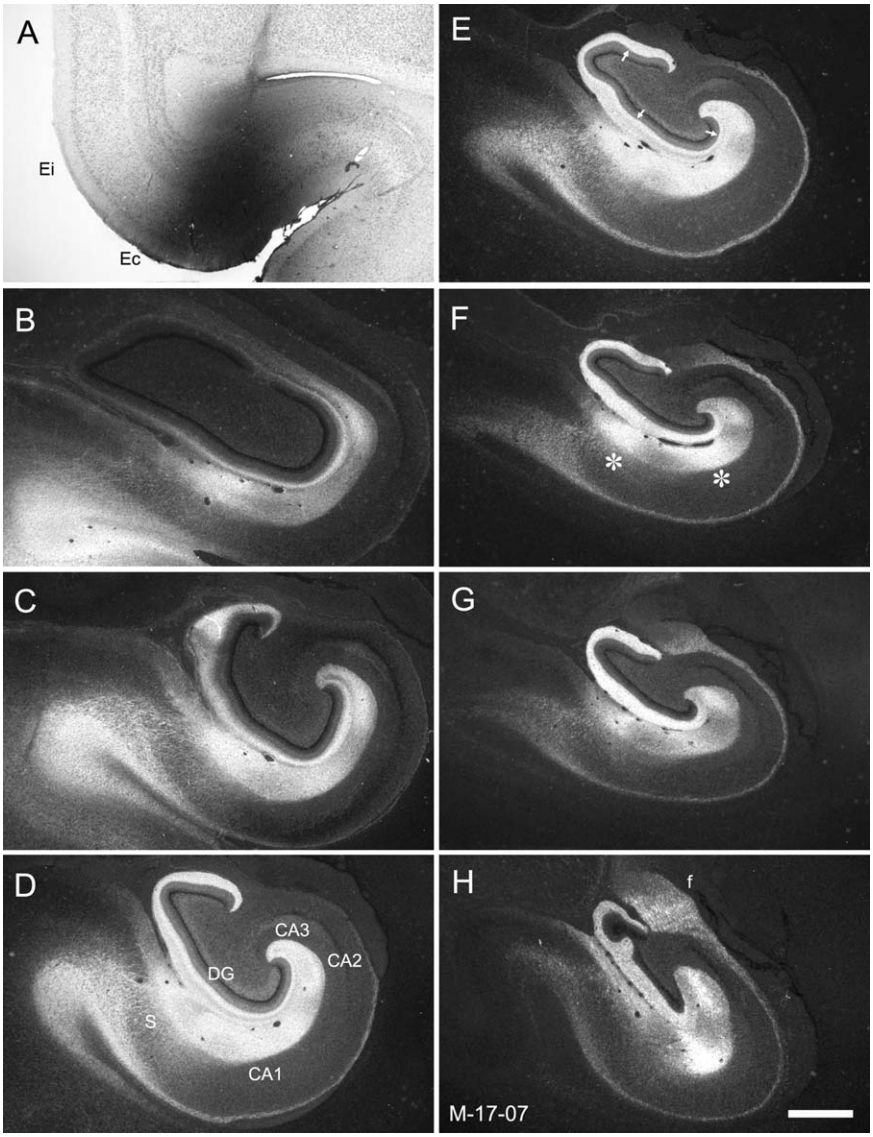

Figure 5. **A:** Brightfield photomicrograph illustrating the ^{3}H-amino acid injection into the lateral aspect of the caudal field (Ec) of the entorhinal cortex in case M-17-07. **B–H:** Darkfield photomicrographs of coronal sections of the 3-week-old infant monkey hippocampal formation arranged from rostral (B) to caudal (H) showing the distribution of anterogradely transported label. Note that labeling extends from the most rostral level of the dentate gyrus (B) to nearly the caudal end (H). The density of labeling is more substantial at mid-rostrocaudal levels (D and E), consistent with the mid-transverse position of the injection site within the entorhinal cortex. Labeling in the molecular layer of the dentate gyrus is distributed throughout the outer two-thirds though the middle third tends to have slightly denser labeling, particularly at rostral and mid-rostrocaudal levels (see arrows in E). Asterisks in F indicate the dense labeling in CA1 and the subiculum that is heaviest at mid-transverse positions of these fields. Note also the substantial number of labeled fibers located in the alveus (D–H, white arrowheads in F). These continue caudally and coalesce in the fimbria at the most caudal levels of the hippocampus (H). For abbreviations, see Figure 1 legend. Scale bar = 1 mm in H (applies to A–H).

(Fig. 7G, asterisks). Differences in the pattern of laminar termination are more clearly seen in Figure 8, which presents higher magnification photomicrographs of the molecular layer of the dentate gyrus in cases M-16-07 and M-20-07. The densest labeling is observed in the outer third of the molecular layer in M-16-07 and in the middle third of the molecular layer in M-20-07.

Commissural projections of the entorhinal cortex

We have previously demonstrated in the adult macaque monkey (Amaral et al., 1984) that the caudal fields of the entorhinal cortex project homotopically to the contralateral entorhinal cortex, where they terminate primarily in layer III. The commissural projection in the neonatal macaque monkey appears to be somewhat

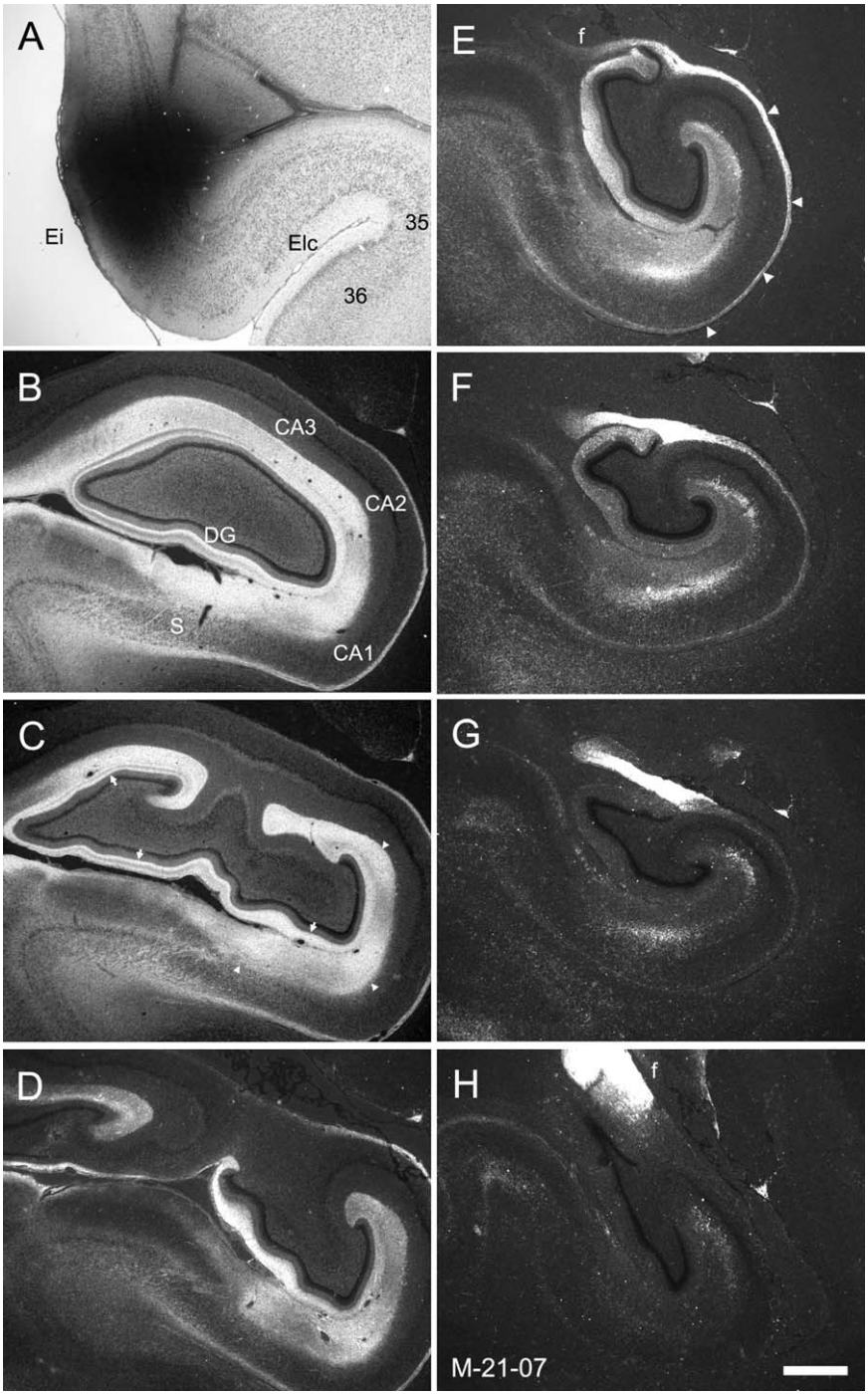

Figure 6. **A:** Brightfield photomicrograph illustrating the injection site in experiment M-21-07 in the medial half of the intermediate field (Ei) of the entorhinal cortex. **B–H:** Darkfield photomicrographs of coronal sections of the infant monkey hippocampal formation arranged from rostral (B) to caudal (H) showing the distribution of anterograde labeling. The injection is approximately at the same level as in case M-17-07, illustrated in Figure 5. However, injection M-21-07 is located medially in Ei. The strongest labeling is present in the rostral part of the dentate gyrus, hippocampus, and subiculum (B and C), and little or no labeling extends into the caudal part of these regions (G and H). As in case M-17-07, the heaviest labeling of the molecular layer of the dentate gyrus is located in the middle third (arrows in C). Note also the very dense bundle of labeled fibers within the alveus (arrowheads in E) that continue into the fimbria. For abbreviations, see Figure 1 legend. Scale bar = 1 mm in H (applies to A–H).

different. First, all ^{3}H-amino acid injections except for the most rostral one (M-16-07) gave rise to very substantial commissural projections to the contralateral entorhinal cortex. Even quite rostral injections, such as case M-8-08, had robust commissural connections. Second, the heaviest terminal labeling in the contralateral

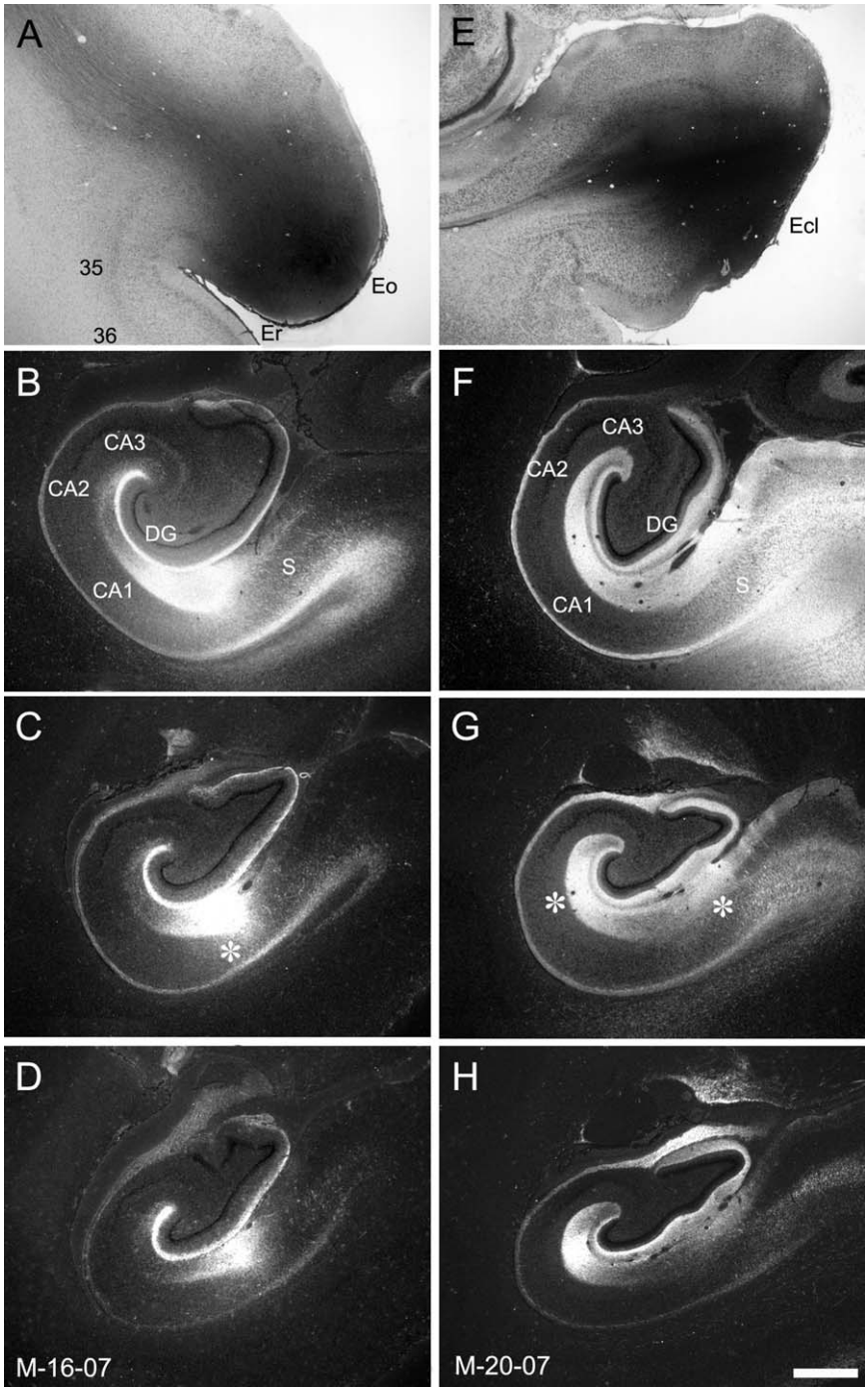

Figure 7. **A,E:** Brightfield photomicrographs of the ^{3}H-amino acid injections in cases M-16-07 (A) and M-20-07 (E). The injection in M-16-07 is near the rostral pole of the entorhinal cortex and involves fields Eo and Er. The injection in case M-20-07 is near the caudal pole of the entorhinal cortex and involves the caudal limiting field (Ecl). **B–D,F–H:** Darkfield photomicrographs of coronal sections of the infant monkey hippocampal formation arranged from rostral (B and F) to caudal (D and H) showing the distribution of anterogradely labeled projections in cases M-16-07 and M-20-07, respectively. In both cases, labeling is distributed extensively through the rostrocaudal extent of the dentate gyrus. However, in M-16-07, the heaviest labeling is in the outer third of the molecular layer of the dentate gyrus, whereas in case M-20-07 labeling is much heavier in the middle third of the molecular layer. Differences are also seen in the topography of the projection to CA1 and the subiculum as indicated by the asterisks in C and G. The rostral injection in M-16-07 leads to labeling at the border of these two fields, whereas the caudal injection in M-20-07 leads to heaviest labeling in CA1 close to CA2 and in the subiculum close to the presubiculum. For abbreviations, see Figure 1 legend. Additional abbreviations: 35 and 36, areas 35 and 36 of the perirhinal cortex. Scale bar = 1 mm in H (applies to A–H).

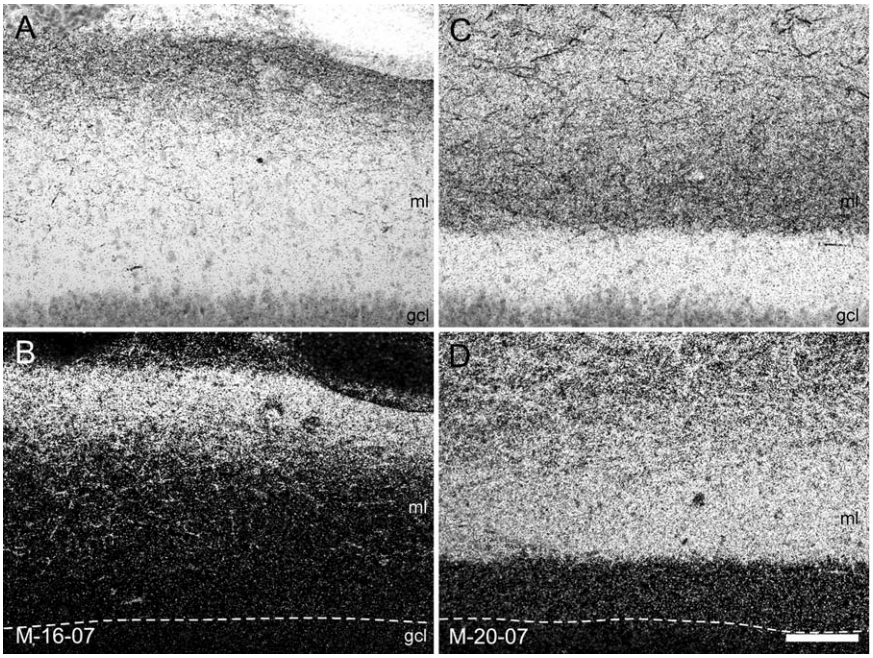

Figure 8. **A–D:** Higher magnification photomicrographs of coronal sections of the same cases illustrated in Figure 7 showing the laminar distribution of anterogradely transported label in the molecular layer (ml) of the dentate gyrus following the tracer injections in the rostral (A and B; case M-16-07, injection in Er/Eo) and caudal (C and D; case M-20-07, injection in Ecl) parts of the entorhinal cortex in infant monkeys. Brightfield photomicrographs (A and C) and darkfield photomicrographs (B and D) show the same location of the molecular layer of the dentate gyrus. Note that labeling is densest in the superficial (A and B) part of the molecular layer in case M-16-07 with the rostral injection (equivalent to a lateral entorhinal area injection in the rodent) and is densest in the mid-portion of the molecular layer (C and D) in case M-20-07, which had an injection into the caudal entorhinal cortex (equivalent to a medial entorhinal area injection in the rodent). In B and D, the border between the molecular layer of the dentate gyrus and the granule cell layer (gcl) is indicated by dashed lines. Scale bar = 100 μm in D (applies to A–D).

entorhinal cortex was consistently in layer I (Fig. 9B,C), although there was additional terminal labeling in layers III–VI. A prominent bundle of fibers traveled within the alveus on the side of the injection (Figs. 5, 6) to enter the ipsilateral fimbria. The fibers crossed the midline in the dorsal hippocampal commissure (Fig. 9A), where they took a similar route to the contralateral entorhinal cortex and then terminated most heavily in layer I (Fig. 9C). We had never observed such a substantial projection to layer I in the adult cases (Amaral et al., 1984).

PHA-L, BDA, and FR injections in the infant entorhinal cortex

Although the ^{3}H-amino acid injections were very useful in showing the overall organization of the entorhinal projections in the neonatal brains, the more discrete tracers (PHA-L, BDA, and FR) were able to elaborate specific facets of the organization of the perforant path projections. There were three PHA-L, six BDA, and four FR injections that successfully involved various rostrocaudal and mediolateral portions of the entorhinal cortex (Fig. 2). Photomicrographs of two of these injections, M-17-07-PHA-L situated rostrally in Er and M-14-05-BDA located caudally in Ec, have been illustrated (Fig. 10A and C, respectively). Overall, the pattern of projections determined with these experiments was very consistent with the ^{3}H-amino acid experiments.

In case M-17-07 (Fig. 11), anterogradely labeled axons traveled within the angular bundle and perforated the subiculum as the perforant path (Fig. 11D). Axons and terminals were distributed to the border region of CA1 and the subiculum (Fig. 11B–F). There was also a clear projection to the molecular layer of the dentate gyrus, with the heaviest fiber and terminal labeling in its outer third.

Figure 12 presents sections at the same rostrocaudal level of the hippocampal formation to compare the topographic distribution of fibers arising from the injections in cases M-17-07 and M-14-05. It is clear that in case M-17-07, axons terminate at the border of CA1 with the subiculum (asterisk in Fig. 12B), whereas in case M-14-05 (Fig. 12D), the projection is directed to a more proximal portion of CA1 (asterisk located closer to CA2) and a more distal portion of the subiculum (asterisk located closer to the presubiculum). The

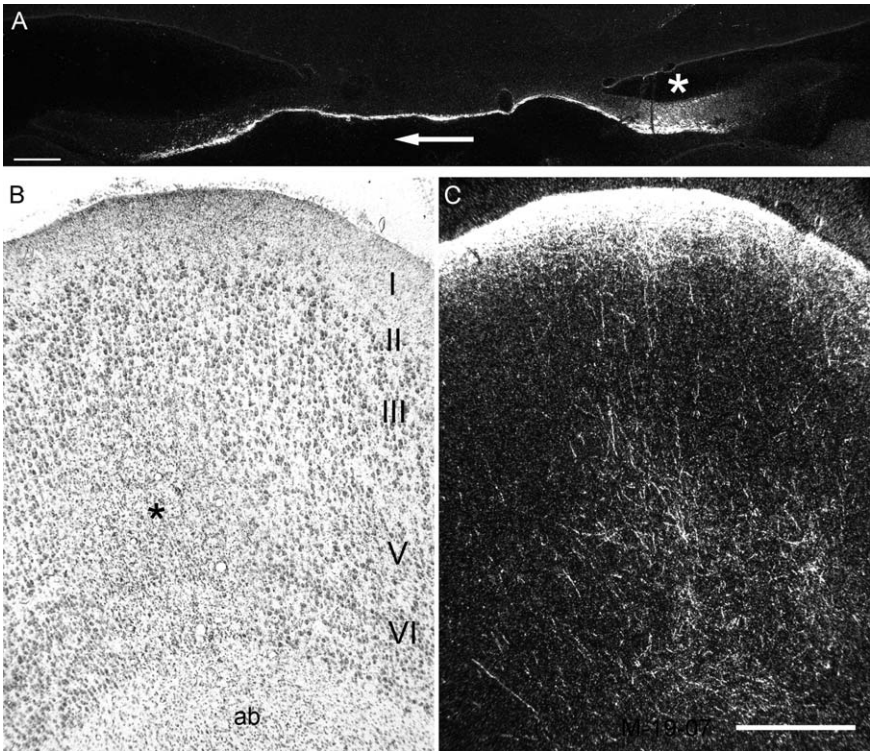

Figure 9. **A:** Darkfield photomicrograph of the fimbria and dorsal hippocampal commissure in case M-19-07. The injection in this case involved the caudal portion of Ei and the rostral part of Ec. A patch of labeled fibers travels in the medial half of the fornix on the side ipsilateral to the injection (white asterisk) and crosses the dorsal hippocampal commissure to enter the contralateral fornix. Fibers travel caudalward to enter the fimbria and then rostrally in the alveus and angular bundle (ab) to reach the homotopic portion of the entorhinal cortex. **B,C:** Brightfield and darkfield photomicrographs, respectively, of the same coronal section through Ec on the side contralateral to the injection site. The photomicrograph in B shows Nissl staining and the various layers of the entorhinal cortex (I-VI). There is also an area of increased gliosis (black asterisk) indicative of a retrograde tracer injection that was placed on this side of the entorhinal cortex. The darkfield photomicrograph in C shows labeled fibers emerging from the angular bundle deep to the entorhinal cortex and terminating primarily in the superficial portion of layer I. Scale bar = 500 μm in A and C (applies to B,C).

laminar organization of the projections arising from these two injections to the molecular layer of the dentate gyrus is more clearly illustrated in Figure 13. Whereas the rostral injection in M-17-07 leads to fiber and terminal labeling in the outer portion of the molecular layer (Fig. 13B), the more caudal injection in case M-14-05 leads to heavier labeling in the middle portion of the molecular layer.

Finally, the more discrete injections provided evidence that the laminar organization of the entorhinal projections to the other hippocampal fields was also established in the newborn. In adults, layer II neurons give rise to projections to the dentate gyrus and CA3, whereas layer III neurons project to CA1 and the subiculum. In case M-15-07, the BDA injection only involved layer III neurons. There were labeled fibers and terminals within the molecular layer of the subiculum and the stratum lacunosum-moleculare of CA1 for nearly the entire rostrocaudal extents of these fields. However, there were no projections into the dentate gyrus or CA3 (data not shown). In case M-11-05, in contrast, the BDA injection mainly involved layer II and gave rise to projections that preferentially innervated the dentate gyrus and CA3.

Varicosities on labeled axons

Labeled axons in the dentate gyrus and hippocampus resulting from injections in the entorhinal cortex demonstrated a variety of diameters, and their varicosities ranged greatly in size. There were many fibers that were thick and nonvaricose and had the appearance of fibers of passage, but the vast majority of fibers were highly varicose (Fig. 14A,B). The size and shape of varicosities had the appearance of presynaptic boutons, but this would need to be confirmed with electron microscopy. Although it was beyond the scope of this initial study to carry out a quantitative evaluation of the density of varicosities in the infant relative to the adult,

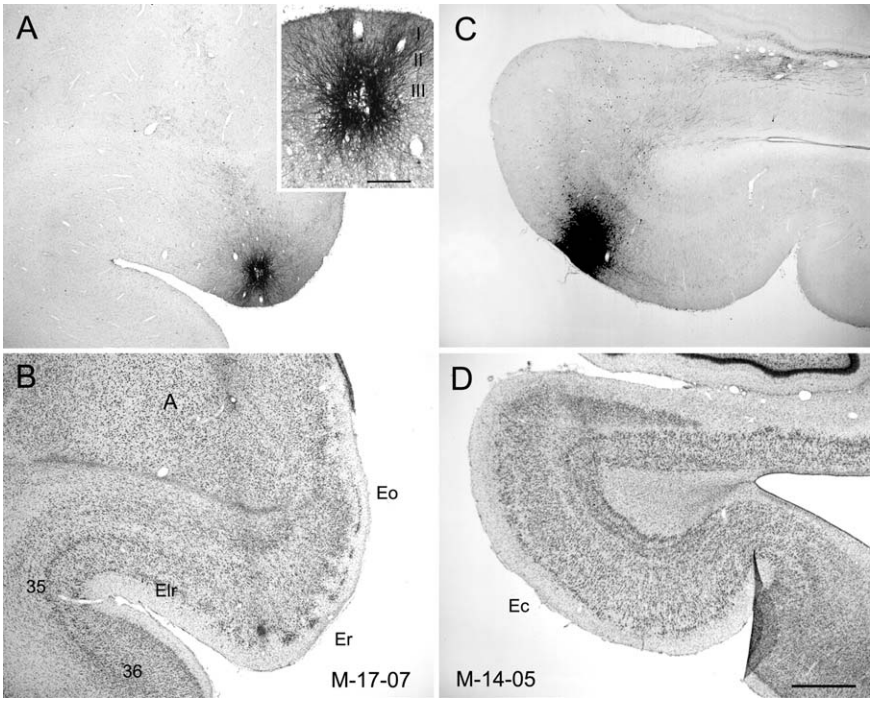

Figure 10. **A,C:** Photomicrographs of coronal sections showing the injection sites of PHA-L (A) and BDA (C) in the entorhinal cortex of infant monkeys. **B,D:** Nissl-stained sections located adjacent to sections in A and C. A: PHA-L injection located in the rostral part of the entorhinal cortex (Er) in case M-17-07. **A, inset:** Injection at higher magnification to demonstrate involvement primarily of layer III and II cells. C: A BDA injection located in the caudal part of the entorhinal cortex (Ec) in case M-14-05 (B) that involves layers I–III. For abbreviations, see Figure 1 legend. Scale bar = 1 mm in D (applies to A–D); 250 μm in inset to A.

to a first approximation, axons looked equally varicose at both ages.

DISCUSSION

The goal of the present study was to evaluate the general level of maturity of the entorhinal cortex projections to the dentate gyrus, hippocampus, and subiculum in the newborn rhesus monkey. This is the first experimental analysis of these projections in the newborn macaque monkey, and thus several fundamental questions required answers. First, does the perforant path project to the expected regions (dentate gyrus, hippocampus, and subiculum) of the rest of the hippocampal formation? The answer to this is clearly yes. There was a consistent finding of substantial perforant path projections in both the ^{3}H-amino acid experiments and with the more discrete tracers such as PHA-L. Second, to what extent is the topographic and laminar organization that is seen in the adult monkey established in the newborn monkey? Again, the answer appears clearly to be that all major features of the topography are observable in the 2-week-old monkey. It is certainly possible that there are quantitative differences between the discreteness of the laminar organization or density of termination between the newborn and the adult. This would certainly be expected for the terminations of the dentate gyrus because there is still substantial neurogenesis that will take place postnatally (Jabes et al., 2010, 2011).

However, what was striking was that all of the topographic and laminar patterns observed in the adult perforant path projections were observed in these neonatal animals. Finally, is there any evidence for exuberant projections in the neonatal perforant path projection at this age? Without more detailed quantitative comparative evaluations of connectivity (which the current tracer experiments would not support), the answer to this question can only be provisional. In general, there was no obvious indication of exuberant projections arising from the entorhinal cortex to the ipsilateral fields of the hippocampal formation. In contrast, the commissural projection of the entorhinal cortex to contralateral homotypical regions was clearly more extensive in the neonate compared with the adult. This projection appears to originate from a much larger rostrocaudal extent of the entorhinal cortex in the neonate. Moreover, the projection to the contralateral side appears to be more substantial than in the adult, and the projection terminates mainly in layer I in the infant,

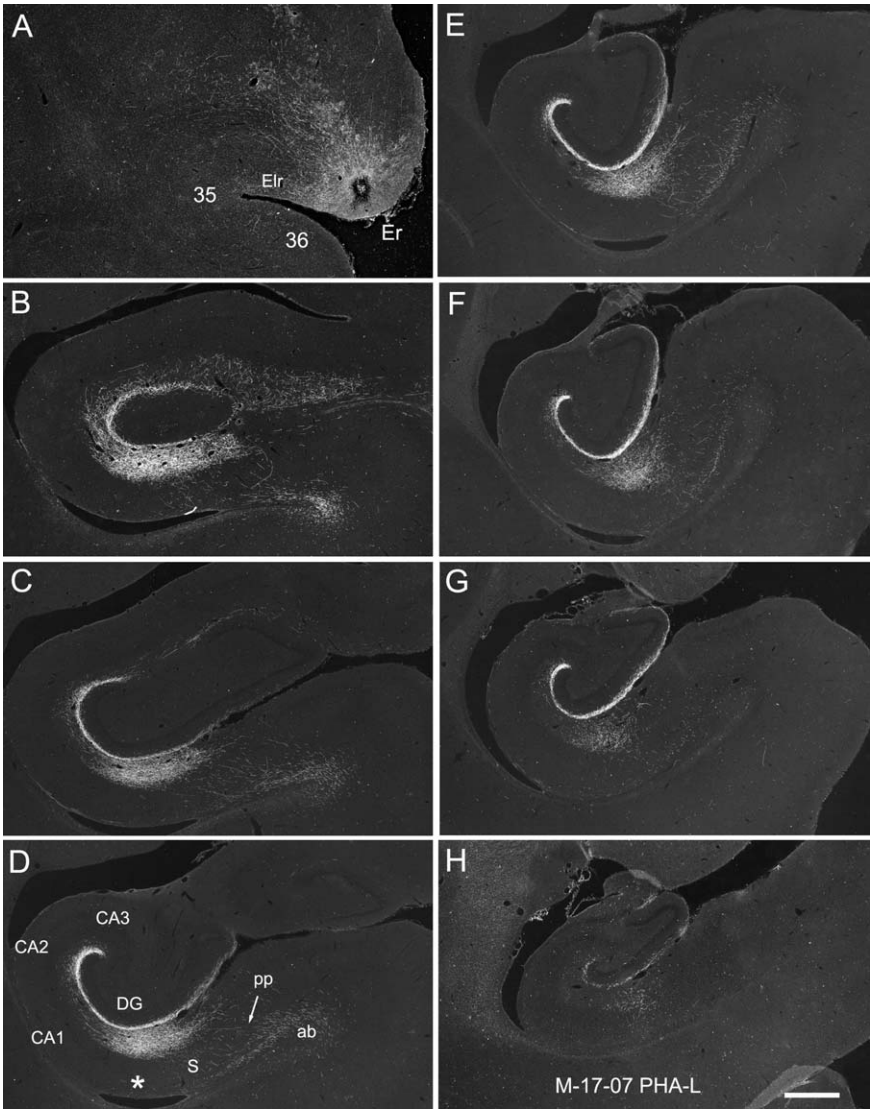

Figure 11. **A–H:** Darkfield photomicrographs illustrating the injection (A) and anterogradely transported label in the hippocampal formation in case M-17-07. A: The PHA-L injection site is rostrally placed and involves primarily layers III and II of the rostral part of the entorhinal cortex (Er). Anterogradely transported fibers travel in the angular bundle (ab in D) traverse the subiculum (S) in the perforant path (pp in D), and innervate the dentate gyrus, CA1, and subiculum. Labeling is very extensive rostrocaudally and extends from near the rostral pole of the dentate gyrus (B) to nearly its caudal end (H). The injection is very rostrally placed, and fibers terminate most heavily in the outer third of the molecular layer of the dentate gyrus and at the border between CA1 and the subiculum (asterisk in D). Scale bar = 1 mm in H (applies to A–H).

whereas it terminates mainly in layer III in the adult. This raises the prospect that a prominent commissural projection established early in brain development is eliminated or modified as the animal matures.

Comparisons with previous studies in adult monkeys

Previous studies in adult monkeys have demonstrated that the medial part of the entorhinal cortex projects preferentially to rostral levels of the dentate gyrus, hippocampus, and subiculum, whereas the more lateral part of the entorhinal cortex projects to more caudal parts of the hippocampal formation (Van Hoesen and Pandya, 1975b; Witter and Amaral, 1991; Witter et al., 1989). We had ample injection sites in the neonatal cases to confirm that this organization is apparent in the 2-week-old hippocampal formation. It has also been demonstrated in the adult monkey that the laminar pattern of termination in the dentate gyrus and CA3 and the transverse pattern of termination in CA1 and the subiculum depend on the rostrocaudal level of the injection site in the entorhinal cortex (Witter and Amaral, 1991). Again, we observed the same organization in the neonatal monkeys.

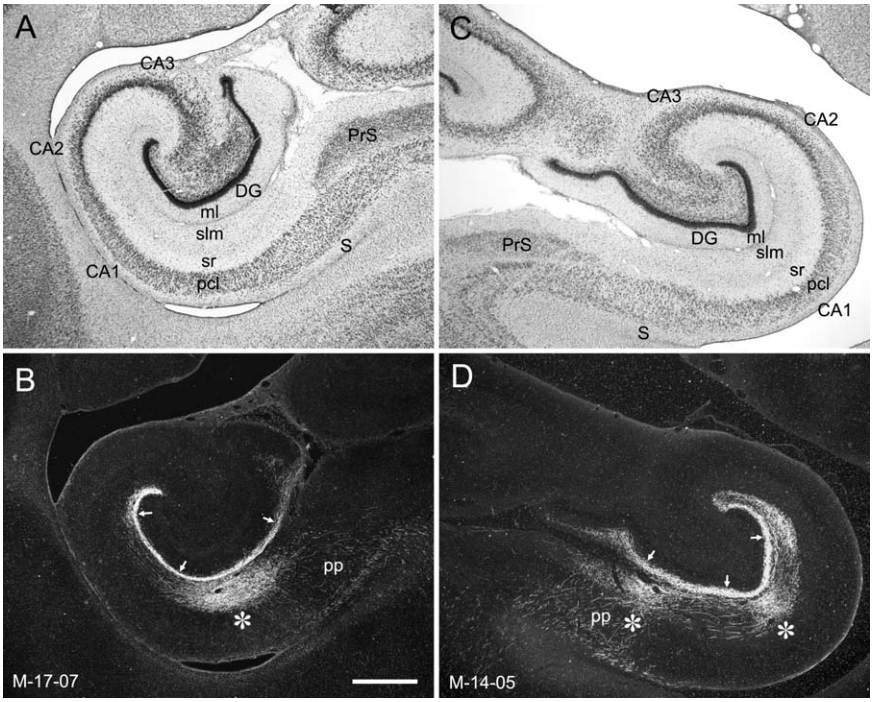

Figure 12. Examples to illustrate the topographic organization of entorhinal projections to the hippocampal formation in the 3-week-old macaque monkey. **A,B:** Brightfield and darkfield, respectively, photomicrographs of a mid-rostrocaudal level from the hippocampal formation in case M-17-07. **C,D:** Brightfield and darkfield, respectively, photomicrographs of a mid-rostrocaudal level from the hippocampal formation in case M-14-05. B: Darkfield photomicrograph of a section adjacent to the one in A showing anterograde labeling after a PHA-L injection in the rostral part of the entorhinal cortex in case M-17-07. D: Darkfield photomicrograph of a section adjacent to the one in C showing anterograde labeling after a BDA injection in the caudal part of the entorhinal cortex in case M-14-05. As is observed in adult monkeys, a rostrally placed injection in neonate monkeys reveals projections that terminate preferentially in the superficial portion of the molecular layer of the dentate gyrus (arrows in B) and at the border of CA1 and the subiculum (asterisk in B). In contrast, a caudally placed injection, such as the one in case M-14-05, reveals projections that terminate more heavily in the middle third of the molecular layer (arrows in D) and away from the CA1/subiculum border (asterisks in D). For abbreviations, see Figure 1 legend. Scale bar = 1 mm in B (applies to A–D).

Although the present study cannot provide definitive evidence as to the laminar organization of the cells of origin of the perforant path projections, we observed that injections confined to layer III gave rise to projections that preferentially terminated in CA1 and the subiculum, whereas injections that predominantly involved layer II terminated in the dentate gyrus and CA3. These results are in good agreement with previous findings in adult monkeys (Witter and Amaral, 1991) that projections to the dentate gyrus and fields CA2 and CA3 originate mainly in layer II of the entorhinal cortex, whereas projections to CA1 and the subiculum originate mainly in layer III (and to a lesser extent from layer V).

Development of entorhinal cortex projections in other species

Much of the work examining the development of the entorhinal cortex projections has been carried out in the mouse (Ceranik et al., 2000; Deng et al., 2006, 2007; Snyder et al., 1991; Super et al., 1998; Super and Soriano, 1994), generally using the lipophilic dyes DiI and DiO. In general, the earliest entorhinal fibers enter the alvear pathway at around fetal day 16. Fibers are seen in the incipient stratum lacunosum-moleculare on fetal day 17 and enter the molecular layer of the dentate gyrus some time between fetal day 19 and postnatal day 2. Importantly, a mature pattern of innervation becomes apparent around postnatal day 10. All the studies carried out in the mouse emphasize that the laminar pattern of termination of the entorhinal fibers is established from the very earliest stages of innervation. It has been proposed that either Cajal-Retzius cells alone (Ceranik et al., 2000) or in combination with γ-aminobutyric acid (GABA)ergic neurons (Super et al., 1998) form an early scaffolding that guides an appropriate laminar termination of the perforant path fibers. Work carried out in the rat using the autoradiographic method (Deng et al., 2006, 2007; Fricke and Cowan, 1977) has also found that perforant path fibers innervate the dentate gyrus quite early (at least by postnatal day 2) and a pattern similar to that in the adult is seen by postnatal day 6.

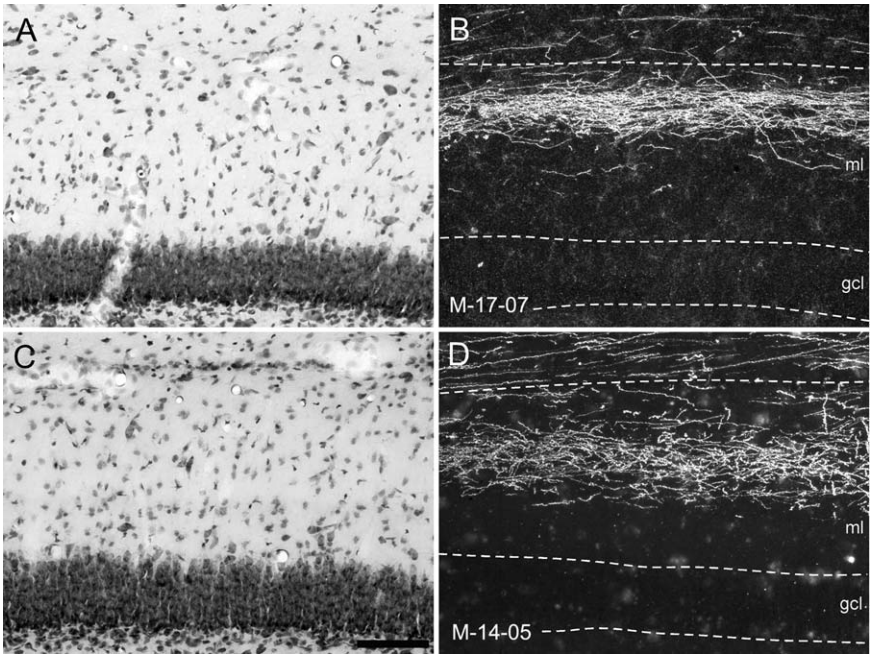

Figure 13. **A–D:** Higher magnification photomicrographs of coronal sections showing the laminar distribution of anterograde labeling in the molecular layer (ml) of the dentate gyrus following the tracer injections in the rostral (B, PHA-L in case M-17-07) and caudal (D, BDA in case M-14-05) parts of the entorhinal cortex in infant monkeys. These are the same cases illustrated at lower magnification in Figure 12. Adjacent Nissl-stained sections for B and D are shown in A and C, respectively. The superficial and deep borders of the molecular layer of the dentate gyrus and the granule cell layer (gcl) are indicated by dashed lines. Note that labeled axons and terminals are preferentially located in the superficial portion of the molecular layer of the dentate gyrus following the rostral injection (B), whereas labeled axons and terminals are preferentially located in the mid-portion of the molecular layer following the caudal injection. Scale bar = 100 μm in C (applies to A–D).

To our knowledge, there are no publications on the development of the perforant path projection in the macaque monkey. However, there has been one preliminary study carried out in human fetal material. Hevner and Kinney (1996) used DiI to evaluate entorhinal cortex projections in human fetal brain from 19 to 22 weeks of gestation. At 19 weeks, projections could routinely be observed between the entorhinal cortex and the subiculum and hippocampus. However, by 22 weeks, the projections to the dentate gyrus and hippocampus were said to have reached only rudimentary levels of development. Interestingly, despite the immature status of the projections at this time, their laminar organization appeared to be typical of the mature projections.

Taken together, available data indicate that the entorhinal cortex projections to the other fields of the hippocampal formation are established fairly early in cortical development. Moreover, from the very earliest stages of innervation of the subiculum, hippocampus, and dentate gyrus, the fibers originating in the entorhinal cortex are organized according to the same laminar pattern that is seen in the mature brain. These findings in rodents and humans are consistent with our results in monkeys. By the second postnatal week in the macaque monkey, all components of the entorhinal cortex projections have been established. Moreover, all topographic and laminar features of the mature projection have been established by this time. It remains to be seen when, in the macaque monkey, entorhinal cortex fibers first enter the developing hippocampus and dentate gyrus, and this will be evaluated in future studies using lipophilic dyes.

It should also be noted that available evidence indicates that other pathways of the macaque monkey hippocampal formation have already been established in the neonatal monkey. The mossy fibers, for example, are clearly present at birth, although they do undergo significant postnatal development (Seress and Ribak, 1995). Based on the presence of calretinin and substance P staining, Berger and colleagues (2001) established that the projections from the supramamillary region of the posterior hypothalamus have innervated the dentate gyrus and CA2 region of the hippocampus by the third trimester of the macaque monkey gestation. Neurochemical staining of major pathways such as the fimbria, fornix, angular bundle, and cingulum bundle suggest that both intrinsic hippocampal pathways and

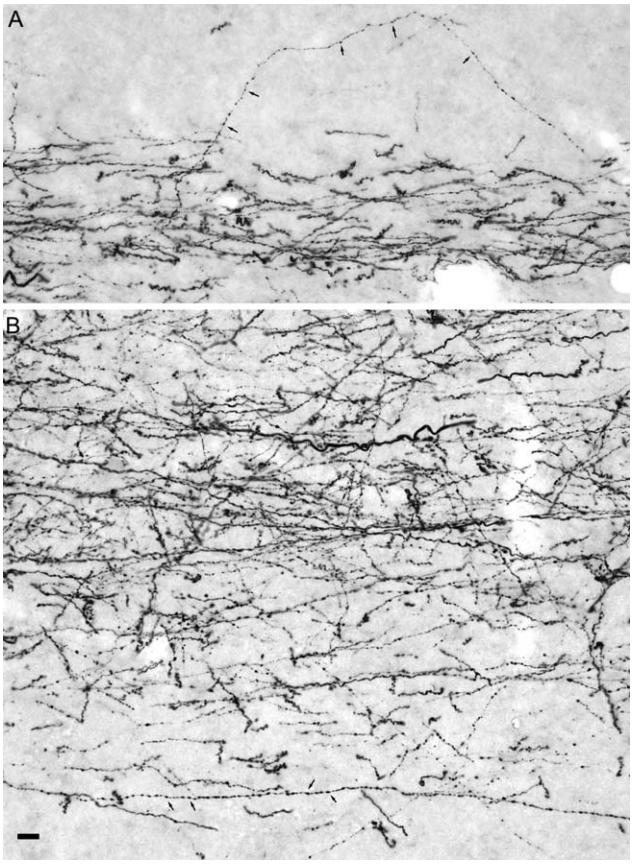

Figure 14. High-magnification brightfield photomicrographs of anterogradely PHA-L– labeled fibers in case M-17-07. **A:** Fibers in the outer portion of the molecular layer of the dentate gyrus. The fibers have a substantial range of thicknesses but virtually all have varicosities (arrows) that are reminiscent of synaptic boutons. **B:** Fibers in stratum lacunosum-moleculare of CA1. Again, fibers range from thick nonvaricose fibers, particularly in the superficial portion of the field, to thinner highly varicose fibers (arrows) in the deeper portion of the field. Scale bar = 10 μm in B (applies to A,B).

those of major afferents and efferents are already established during late fetal life (Berger et al., 1997).

Functional considerations

We have shown that the pattern of projections from the entorhinal cortex to the other hippocampal fields is not only established in the newborn macaque monkey, but that it bears striking resemblance to the topographical and laminar organization observed in the adult monkey. What are the implications of these findings for the ontogeny of hippocampal-based memory? This topic has recently been taken up in great detail by Lavenex and Banta Lavenex (2013), who have sought to integrate neuroanatomical, genetic, and behavioral data to present a coherent hypothesis on the relationship between hippocampal development and the emergence of components of hippocampal function. We shall present a much abbreviated discussion of some of the implications of the data on the development of entorhinal cortex projections. It is also important to bear in mind that findings from the macaque monkey may not be entirely representative of the trajectory of hippocampal development in the human brain. How good of a model the macaque monkey is for human hippocampal development remains to be determined.

On the one hand, it is important to remember that the presence of a connection from one brain region to another does not necessarily imply that the connection is functional. Levitt and colleagues, for example (Rinaman et al. (2000)), have used the transneuronal transport of pseudorabies virus to demonstrate that functional connections between the lateral hypothalamic area and the amygdala with neurons of the medullary dorsal vagal complex are established several days after axons have entered this region. Therefore, even though we have shown innervation by entorhinal fibers to all known terminal fields in the hippocampal formation, the magnitude of functional connectivity has not been addressed. In fact, we know that at 2 weeks of age it must be far less than in the mature animals. The best evidence for this is that, as we have reported previously in monkeys (Jabes et al., 2010, 2011), 40% of the granule cells found in the adult dentate gyrus are generated postnatally, with a peak of generation (about 25%) from birth to 3 months of age. Thus, the fact that perforant path fibers enter the molecular layer of the dentate gyrus does not mean that this connection is functioning as in the mature monkey.

On the other hand, there is certainly evidence that the circuits we have described are at least partially functional at birth. In seminal electron microscopic studies carried out by Eckenhoff and Rakic (1991), they found that synaptogenesis in the macaque monkey dentate gyrus progressed rapidly during the last half of gestation. They also reported a continued increase in synapse formation postnatally that is consistent with the addition of more granule cells to the dentate gyrus and the maturation of granule cell dendrites that is taking place during the first 6 months of life. This is consistent with our observation that the perforant path fibers were highly varicose in our preparations, presumably an indication of presynaptic boutons. Total dendritic length of granule cells in newborn macaque monkeys is about 1.3 mm (Duffy and Rakic, 1983), whereas mature dentate granule cells are on the order of 2 mm (Seress, 2007). So, the postnatal period is characterized both by increased numbers of granule cells and by increased maturation of the dendritic trees of individual granule cells.

Finally, in a remarkable series of experiments, Khazipov et al. (2001) carried out electrophysiological and morphological studies of hippocampal slices obtained from fetal *Macaca fascicularis* monkeys. They found that both GABAergic and glutamatergic neurotransmission rapidly evolved over the second half of gestation and that epileptiform activity could be induced with the $GABA_A$ receptor antagonist bicuculline by the last third of gestation. These electrophysiological indications of functional circuits emerged in parallel with the development of synaptic spines on CA1 and CA3 pyramidal cells, which increased from very few spines per cell around 100 days of gestation to 7,000 spines per neuron around birth (at 165 days of gestation). The adult estimate would be on the order of 20,000 spines in the mature monkey (Altemus et al., 2005).

Taken together, these data indicate that the topographical organization of the primate hippocampal formation circuitry is established by birth, but that there is continued refinement of many aspects of hippocampal connectivity, at least for many months after birth (Favre et al., 2012a,b; Jabes et al., 2010, 2011; Lavenex et al., 2011). Accumulating evidence suggests that the differential maturation of distinct hippocampal circuits contributes to the emergence of different "hippocampus-dependent" memory processes over the course of postnatal development (Lavenex and Lavenex Banta, 2013). Thus, factors that affect hippocampal development at any point during this period could have serious consequences for normal cognitive development (Ribordy et al., 2013) and for the emergence of neurodevelopmental conditions such as schizophrenia (Favre et al., 2012a).

ACKNOWLEDGMENTS

The authors thank Jeffery L. Bennett, Kelly C. Brown, and Alicja Omanska-Klusek for surgical and tissue processing assistance; Pamela Banta Lavenex for surgical assistance; and Megan N. Anderson, Jose D. Rosa, and John Sylvain for tissue processing assistance.

CONFLICT OF INTEREST STATEMENT

The authors declare that they have no conflicts of interest with this work.

ROLE OF AUTHORS

All authors had full access to all the data in the study and take responsibility for the integrity of the data and the accuracy of the data analysis. Study concept and design: DGA. Acquisition of data: DGA, PL, and HK. Analysis and interpretation of data: DGA, PL, and HK. Drafting of the manuscript: DGA. Critical revision of the manuscript for important intellectual content: DGA, PL. Obtained funding: DGA, PL. Administrative, technical, and material support: DGA, PL. Study supervision: DGA.

LITERATURE CITED

Altemus KL, Lavenex P, Ishizuka N, Amaral DG. 2005. Morphological characteristics and electrophysiological properties of CA1 pyramidal neurons in macaque monkeys. Neuroscience 136:741–756.

Amaral DG, Lavenex P. 2007. Hippocampal neuroanatomy. In: Andersen P, Morris R, Amaral D, Bliss T, O'Keefe J, editors. The hippocampus book. New York: Oxford University Press. p 37–114.

Amaral DG, Price JL. 1983. An air pressure system for the injection of tracer substances into the brain. J Neurosci Methods 9:35–43.

Amaral DG, Witter MP. 1989. The three-dimensional organization of the hippocampal formation: a review of anatomical data. Neuroscience 31:571–591.

Amaral DG, Insausti R, Cowan WM. 1984. The commissural connections of the monkey hippocampal formation. J Comp Neurol 224:307–336.

Amaral DG, Insausti R, Cowan WM. 1987. The entorhinal cortex of the monkey: I. Cytoarchitectonic organization. J Comp Neurol 264:326–355.

Berger B, Alvarez C, Pelaprat D. 1997. Retrosplenial/presubicular continuum in primates: a developmental approach in fetal macaques using neurotensin and parvalbumin as markers. Brain Res Dev Brain Res 101:207–224.

Berger B, Esclapez M, Alvarez C, Meyer G, Catala M. 2001. Human and monkey fetal brain development of the supramammillary-hippocampal projections: a system involved in the regulation of theta activity. J Comp Neurol 429:515–529.

Blackstad TW. 1958. On the termination of some afferents to the hippocampus and fascia dentata; an experimental study in the rat. Acta Anat (Basel) 35:202–214.

Ceranik K, Zhao S, Frotscher M. 2000. Development of the entorhino-hippocampal projection: guidance by Cajal-Retzius cell axons. Ann N Y Acad Sci 911:43–54.

Chrobak JJ, Amaral DG. 2007. Entorhinal cortex of the monkey: VII. intrinsic connections. J Comp Neurol 500: 612–633.

Cowan WM, Gottlieb DI, Hendrickson AE, Price JL, Woolsey TA. 1972. The autoradiographic demonstration of axonal connections in the central nervous system. Brain Res 37: 21–51.

Deng JB, Yu DM, Li MS. 2006. Formation of the entorhino-hippocampal pathway: a tracing study in vitro and in vivo. Neurosci Bull 22:305–314.

Deng JB, Yu DM, Wu P, Li MS. 2007. The tracing study of developing entorhino-hippocampal pathway. Int J Dev Neurosci 25:251–258.

Dolorfo CL, Amaral DG. 1998. Entorhinal cortex of the rat: topographic organization of the cells of origin of the perforant path projection to the dentate gyrus. J Comp Neurol 398:25–48.

Duffy CJ, Rakic P. 1983. Differentiation of granule cell dendrites in the dentate gyrus of the rhesus monkey: a quantitative Golgi study. J Comp Neurol 214:224–237.

Eckenhoff MF, Rakic P. 1991. A quantitative analysis of synaptogenesis in the molecular layer of the dentate gyrus in the rhesus monkey. Brain Res Dev Brain Res 64: 129–135.

Favre G, Banta Lavenex P, Lavenex P. 2012a. Developmental regulation of expression of schizophrenia susceptibility

genes in the primate hippocampal formation. Translational psychiatry 2:e173.
Favre G, Banta Lavenex P, Lavenex P. 2012b. miRNA regulation of gene expression: a predictive bioinformatics analysis in the postnatally developing monkey hippocampus. PloS One 7:e43435.
Fricke R, Cowan WM. 1977. An autoradiographic study of the development of the entorhinal and commissural afferents to the dentate gyrus of the rat. J Comp Neurol 173:231–250.
Hevner RF, Kinney HC. 1996. Reciprocal entorhinal-hippocampal connections established by human fetal midgestation. J Comp Neurol 372:384–394.
Hjorth-Simonsen A, Jeune B. 1972. Origin and termination of the hippocampal perforant path in the rat studied by silver impregnation. J Comp Neurol 144:215–232.
Ino T, Kaneko T, Mizuno N. 1998. Direct projections from the entorhinal cortical layers to the dentate gyrus, hippocampus, and subicular complex in the cat. Neurosci Res 32: 241–265.
Insausti R, Amaral DG. 2008. Entorhinal cortex of the monkey: IV. Topographical and laminar organization of cortical afferents. J Comp Neurol 509:608–641.
Jabes A, Lavenex PB, Amaral DG, Lavenex P. 2010. Quantitative analysis of postnatal neurogenesis and neuron number in the macaque monkey dentate gyrus. Eur J Neurosci 31:273–285.
Jabes A, Lavenex PB, Amaral DG, Lavenex P. 2011. Postnatal development of the hippocampal formation: a stereological study in macaque monkeys. J Comp Neurol 519: 1051–1070.
Khazipov R, Esclapez M, Caillard O, Bernard C, Khalilov I, Tyzio R, Hirsch J, Dzhala V, Berger B, Ben-Ari Y. 2001. Early development of neuronal activity in the primate hippocampus in utero. J Neurosci 21:9770–9781.
Kostovic I, Petanjek Z, Judas M. 1993. Early areal differentiation of the human cerebral cortex: entorhinal area. Hippocampus 3:447–458.
Lavenex P, Amaral DG. 2000. Hippocampal-neocortical interaction: a hierarchy of associativity. Hippocampus 10: 420–430.
Lavenex P, Lavenex PB. 2006. Spatial relational memory in 9-month-old macaque monkeys. Learn Mem 13:84–96.
Lavenex P, Lavenex Banta P. 2013. Building hippocampal circuits to learn and remember: insights into the development of human memory. Behav Brain Res (accepted).
Lavenex P, Suzuki WA, Amaral DG. 2002. Perirhinal and parahippocampal cortices of the macaque monkey: projections to the neocortex. J Comp Neurol 447:394–420.
Lavenex P, Suzuki WA, Amaral DG. 2004. Perirhinal and parahippocampal cortices of the macaque monkey: intrinsic projections and interconnections. J Comp Neurol 472:371–394.
Lavenex P, Banta Lavenex P, Amaral DG. 2007. Postnatal development of the primate hippocampal formation. Dev Neurosci 29:179–192.
Lavenex P, Lavenex PB, Bennett JL, Amaral DG. 2009. Postmortem changes in the neuroanatomical characteristics of the primate brain: hippocampal formation. J Comp Neurol 512:27–51.
Lavenex P, Sugden SG, Davis RR, Gregg JP, Lavenex PB. 2011. Developmental regulation of gene expression and astrocytic processes may explain selective hippocampal vulnerability. Hippocampus 21:142–149.
Mohedano-Moriano A, Pro-Sistiaga P, Arroyo-Jimenez MM, Artacho-Perula E, Insausti AM, Marcos P, Cebada-Sanchez S, Martinez-Ruiz J, Munoz M, Blaizot X, Martinez-Marcos A, Amaral DG, Insausti R. 2007. Topographical and laminar distribution of cortical input to the monkey entorhinal cortex. J Anat 211:250–260.
Mohedano-Moriano A, Martinez-Marcos A, Pro-Sistiaga P, Blaizot X, Arroyo-Jimenez MM, Marcos P, Artacho-Perula E, Insausti R. 2008. Convergence of unimodal and polymodal sensory input to the entorhinal cortex in the fascicularis monkey. Neuroscience 151:255–271.
Pitkanen A, Amaral DG. 1993. Distribution of parvalbumin-immunoreactive cells and fibers in the monkey temporal lobe: the hippocampal formation. J Comp Neurol 331:37–74.
Ribordy F, Jabes A, Banta Lavenex P, Lavenex P. 2013. Development of allocentric spatial memory abilities in children from 18 months to 5 years of age. Cogn Psychol 66:1–29.
Rinaman L, Levitt P, Card JP. 2000. Progressive postnatal assembly of limbic-autonomic circuits revealed by central transneuronal transport of pseudorabies virus. J Neurosci 20:2731–2741.
Ruth RE, Collier TJ, Routtenberg A. 1982. Topography between the entorhinal cortex and the dentate septotemporal axis in rats: I. Medial and intermediate entorhinal projecting cells. J Comp Neurol 209:69–78.
Ruth RE, Collier TJ, Routtenberg A. 1988. Topographical relationship between the entorhinal cortex and the septotemporal axis of the dentate gyrus in rats: II. Cells projecting from lateral entorhinal subdivisions. J Comp Neurol 270:506–516.
Seress L. 2007. Comparative anatomy of the hippocampal dentate gyrus in adult and developing rodents, non-human primates and humans. Prog Brain Res 163:23–41.
Seress L, Ribak CE. 1995. Postnatal development of CA3 pyramidal neurons and their afferents in the Ammon's horn of rhesus monkeys. Hippocampus 5:217–231.
Snyder DC, Coltman BW, Muneoka K, Ide CF. 1991. Mapping the early development of projections from the entorhinal cortex in the embryonic mouse using prenatal surgery techniques. J Neurobiol 22:897–906.
Squire LR, Stark CE, Clark RE. 2004. The medial temporal lobe. Annu Rev Neurosci 27:279–306.
Steward O. 1976. Topographic organization of the projections from the entorhinal area to the hippocampal formation of the rat. J Comp Neurol 167:285–314.
Steward O, Scoville SA. 1976. Cells of origin of entorhinal cortical afferents to the hippocampus and fascia dentata of the rat. J Comp Neurol 169:347–370.
Super H, Soriano E. 1994. The organization of the embryonic and early postnatal murine hippocampus. II. Development of entorhinal, commissural, and septal connections studied with the lipophilic tracer DiI. J Comp Neurol 344:101–120.
Super H, Martinez A, Del Rio JA, Soriano E. 1998. Involvement of distinct pioneer neurons in the formation of layer-specific connections in the hippocampus. J Neurosci 18: 4616–4626.
Suzuki WA, Amaral DG. 1994. Topographic organization of the reciprocal connections between the monkey entorhinal cortex and the perirhinal and parahippocampal cortices. J Neurosci 14:1856–1877.
Tamamaki N. 1997. Organization of the entorhinal projection to the rat dentate gyrus revealed by DiI anterograde labeling. Exp Brain Res 116:250–258.
Tamamaki N, Nojyo Y. 1993. Projection of the entorhinal layer II neurons in the rat as revealed by intracellular pressure-injection of neurobiotin. Hippocampus 3:471–480.
van Groen T, van Haren FJ, Witter MP, Groenewegen HJ. 1986. The organization of the reciprocal connections between the subiculum and the entorhinal cortex in the cat: I. A neuroanatomical tracing study. J Comp Neurol 250:485–497.
van Groen T, Miettinen P, Kadish I. 2003. The entorhinal cortex of the mouse: organization of the projection to the hippocampal formation. Hippocampus 13:133–149.

Van Hoesen G, Pandya DN. 1975a. Some connections of the entorhinal (area 28) and perirhinal (area 35) cortices of the rhesus monkey. I. Temporal lobe afferents. Brain Res 95:1–24.

Van Hoesen GW, Pandya DN. 1975b. Some connections of the entorhinal (area 28) and perirhinal (area 35) cortices of the rhesus monkey. III. Efferent connections. Brain Res 95:39–59.

Van Hoesen GW, Pandya DN, Butters N. 1972. Cortical afferents to the entorhinal cortex of the Rhesus monkey. Science 175:1471–1473.

Witter MP. 1993. Organization of the entorhinal-hippocampal system: a review of current anatomical data. Hippocampus 3:33–44.

Witter MP. 2007. The perforant path: projections from the entorhinal cortex to the dentate gyrus. Prog Brain Res 163C:43–61.

Witter MP, Amaral DG. 1991. Entorhinal cortex of the monkey: V. Projections to the dentate gyrus, hippocampus, and subicular complex. J Comp Neurol 307:437–459.

Witter MP, Groenewegen HJ. 1984. Laminar origin and septotemporal distribution of entorhinal and perirhinal projections to the hippocampus in the cat. J Comp Neurol 224: 371–385.

Witter MP, Griffioen AW, Jorritsma-Byham B, Krijnen JL. 1988. Entorhinal projections to the hippocampal CA1 region in the rat: an underestimated pathway. Neurosci Lett 85: 193–198.

Witter MP, Van Hoesen GW, Amaral DG. 1989. Topographical organization of the entorhinal projection to the dentate gyrus of the monkey. J Neurosci 9:216–228.

Wyss JM. 1981. An autoradiographic study of the efferent connections of the entorhinal cortex in the rat. J Comp Neurol 199:495–512.